THE GEOLOGICAL SOCIETY OF AMERICA®

Middle Eocene CO_2 and climate reconstructed from the sediment fill of a subarctic kimberlite maar

Alexander P. Wolfe[1], Alberto V. Reyes[2]*, Dana L. Royer[3], David R. Greenwood[4], Gabriela Doria[3,5], Mary H. Gagen[6], Peter A. Siver[7], and John A. Westgate[8]

[1]Department of Biological Sciences, University of Alberta, Edmonton, Alberta T6G 2E9, Canada
[2]Department of Earth and Atmospheric Sciences, University of Alberta, Edmonton, Alberta T6G 2E3, Canada
[3]Department of Earth and Environmental Sciences, Wesleyan University, Middletown, Connecticut 06459, USA
[4]Department of Biology, Brandon University, Brandon, Manitoba R7A 6A9, Canada
[5]Department of Plant Sciences, University of Cambridge, Cambridge CB2 3EA, UK
[6]Department of Geography, Swansea University, Singleton Park, Swansea SA2 8PP, UK
[7]Department of Botany, Connecticut College, New London, Connecticut 06320, USA
[8]Department of Earth Sciences, University of Toronto, Toronto, Ontario M5S 3B1, Canada

ABSTRACT

Eocene paleoclimate reconstructions are rarely accompanied by parallel estimates of CO_2 from the same locality, complicating assessment of the equilibrium climate response to elevated CO_2. We reconstruct temperature, precipitation, and CO_2 from latest middle Eocene (ca. 38 Ma) terrestrial sediments in the posteruptive sediment fill of the Giraffe kimberlite in subarctic Canada. Mutual climatic range and oxygen isotope analyses of botanical fossils reveal a humid-temperate forest ecosystem with mean annual temperatures (MATs) more than 17 °C warmer than present and mean annual precipitation ~4× present. *Metasequoia* stomatal indices and gas-exchange modeling produce median CO_2 concentrations of ~630 and ~430 ppm, respectively, with a combined median estimate of ~490 ppm. Reconstructed MATs are more than 6 °C warmer than those produced by Eocene climate models forced at 560 ppm CO_2. Estimates of regional climate sensitivity, expressed as ΔMAT per CO_2 doubling above preindustrial levels, converge on a value of ~13 °C, underscoring the capacity for exceptional polar amplification of warming and hydrological intensification under modest CO_2 concentrations once both fast and slow feedbacks become expressed.

INTRODUCTION

Efforts to understand climate response to sustained greenhouse gas forcing commonly focus on periods of peak Cenozoic warmth during the Paleocene–Eocene thermal maximum and early Eocene (e.g., Zachos et al., 2008; Lunt et al., 2012a). The subsequent cooling trend of the middle and late Eocene (Pagani et al., 2005) is also relevant because atmospheric CO_2 concentrations dovetail the range projected for the coming century (Maxbauer et al., 2014; Jagniecki et al., 2015; Anagnostou et al., 2016; Steinthorsdottir et al., 2016), ultimately crossing the threshold necessary to maintain continental ice sheets (~500 ppm; Royer, 2006). Observations from the Arctic Ocean suggest that ice rafting may have been initiated by the middle Eocene (e.g., Tripati et al., 2008), in apparent conflict with the warmth implied by the terrestrial biota (e.g., Eberle and Greenwood, 2012). Climate models struggle with these critical early Cenozoic intervals because unrealistically high CO_2 forcing is required to produce the temperature responses implied by proxies, particularly for the sparse network of terrestrial high-latitude sites (Lunt et al., 2012a). Furthermore, paleoclimate and CO_2 reconstructions are not commonly derived from the same sedimentary archive; this complicates assessment of proxy-model mismatch and frustrates efforts to understand the sensitivity of past equilibrium climate response to greenhouse gas forcing.

Our objective is to assess climate and greenhouse-gas forcing for Northern Hemisphere subarctic latitudes during the latest middle Eocene by exploiting a remarkable terrestrial sedimentary archive. The Giraffe kimberlite locality (paleolatitude ~63°N) comprises the posteruptive sedimentary fill of a maar formed when kimberlite intruded Precambrian cratonic rocks of the Slave Province at 47.8 ± 1.4 Ma (Creaser et al., 2004). Pollen, $\delta^{18}O$ from wood cellulose, and foliar stomata from this locality provide a comprehensive reconstruction of late middle Eocene climate and CO_2 for the northern subarctic latitudes.

RESULTS

Exploration drill core BHP 99-01 (see Appendix DR1 in the GSA Data Repository[1]) captures ≥50 vertical-equivalent meters of lacustrine sediment overlain by 32 m of peat (Fig. 1), together representing the progressive

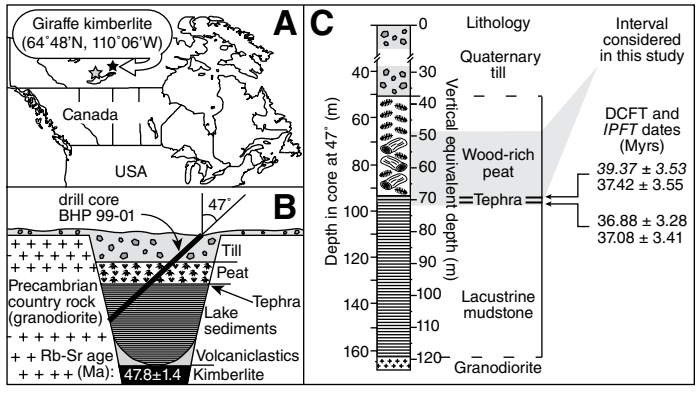

Figure 1. A: Location of the Giraffe kimberlite in the Slave Province, Northwest Territories, Canada. Gray star indicates Yellowknife, the location of the nearest climate station. B: Schematic cross section of posteruptive sedimentary fill and the position of BHP core 99-01 and key stratigraphic features (arrows). C: Core stratigraphy showing the investigated section directly above tephra horizons dated by isothermal plateau (IPFT) and diameter-corrected (DCFT) glass fission track analyses (1σ uncertainty).

[1]GSA Data Repository item 2017202, detailed methods (Appendix DR1), data tables (Tables DR1–DR5) and supplementary Figures DR1–DR5, is available online at http://www.geosociety.org/datarepository/2017 or on request from editing@geosociety.org.

E-mail: areyes@ualberta.ca

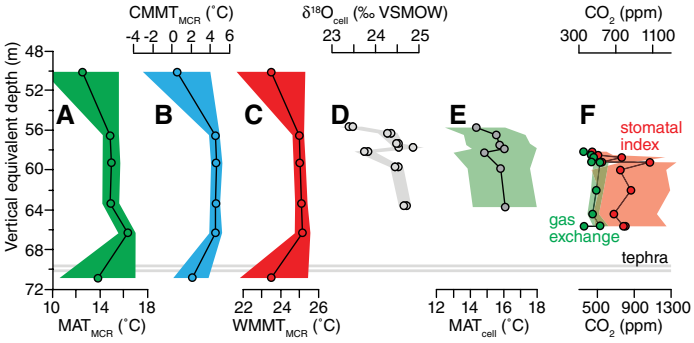

Figure 2. Stratigraphy of climate proxies from the Giraffe peat section. Gray horizontal lines indicate tephra beds. Shading denotes 16th to 84th percentile ranges from Monte Carlo resampling (A, B, C, E, F) and one standard deviation of duplicate isotope analyses (D). A: Mean annual temperature inferred from mutual climatic range (MCR) analysis of pollen types (MAT$_{MCR}$). B: Coldest month mean temperature (CMMT$_{MCR}$). C: Warmest month mean temperature (WMMT$_{MCR}$). D: Wood cellulose $\delta^{18}O_{cell}$ (analytical uncertainty is ~0.3‰; VSMOW—Vienna Standard Mean Ocean Water). E: Median MAT$_{cell}$ inferred from a leaf-water model and Eocene $\delta^{18}O$-MAT transfer function (Appendix DR1 [see footnote 1]). F: Median CO$_2$ concentrations derived from *Metasequoia* stomatal indices (red) and a gas-exchange model (green).

infilling of the maar basin. Both facies have remarkable preservation of aquatic and terrestrial plant fossils (Wolfe et al., 2006; Doria et al., 2011). We analyzed a 21 m section (vertical equivalent depth) of peat in core BHP 99-01, representing ~20 k.y. assuming reasonable accumulation rates and only moderate compaction. The common sampling interval over which we estimate the mean climate state and CO$_2$ concentration includes multiple samples from 7 m of vertical equivalent thickness (Fig. 2), or ~7 k.y. of continuous deposition. Two rhyolitic tephra beds are present in the core directly below the lacustrine-to-peat transition (Fig. 1C). Glass fission track dating (Westgate et al., 2013) of both tephra beds gives a weighted mean age (±1σ) of 37.84 ± 1.99 Ma (Table DR1 and Appendix DR1).

Paleoclimate of the Latest Middle Eocene Subarctic

Pollen assemblages from Giraffe sediments are well preserved, diverse, and include numerous extant North American taxa (Fig. DR1). The relative abundance of angiosperm pollen (53%–74%) is higher than that of gymnosperms throughout the section (Fig. DR2). The former is strongly dominated by fagalean types (*Quercoidites*, *Castanea*, and *Corylus*), with lesser contributions from *Ulmipollenites*, Ericalean taxa, and the Eocene indicators *Platycarya swasticoides* and *Pistillopollenites mcgregorii*. Conifer pollen is strongly dominated by Cupressaceae, for which *Metasequoia* is likely the dominant source given the presence of well-preserved foliage and wood of this taxon (Fig. DR1). Pollen of *Pinus* and *Picea* is distributed throughout the section, whereas that of *Ginkgo*, *Sciadopitys*, and *Tsuga* occurs in trace amounts.

Mutual climate range (MCR) analysis (e.g., Ballantyne et al., 2010; Thompson et al., 2012; see the methods description in Appendix DR1) of these pollen assemblages using nearest living relatives yields reconstructed mean annual temperatures (MATs) of 12.5–16.3 °C (mean ± 1σ = 14.5 ± 1.3 °C), coldest month mean temperatures (CMMTs) of 0.5–4.5 °C (3.4 ± 1.7 °C), and warmest month mean temperatures (WMMTs) of 23.5–25.0 °C (24.5 ± 0.8 °C) (Figs. 2A–2C; Table DR2). Reconstructed mean annual precipitation (MAP) ranges from 1257 to 1292 mm, with a mean uncertainty of 310 mm. The present-day climate for Yellowknife (62.45°N, 114.40°W), the nearest long-term climate station situated 300 km southwest of the Giraffe locality, has a MAT of –4.3 °C, CMMT of -25.6 °C, WMMT of 17.0 °C, and MAP of 289 mm (1981–2010 climate normals; htpp://climate.weather.gc.ca). Thus, middle Eocene MATs were 17–20 °C warmer, CMMTs 27–31 °C warmer, WMMTs 7–8 °C warmer, and MAP 3–5 times higher than present. The North American location with a modern climatology that most closely matches the reconstructed paleoclimate for the Giraffe locality is 3500 km to the southeast at Nashville (Tennessee, USA), with MAT of 15.2 °C, CMMT of 3.2 °C, WMMT of 26.3 °C, and MAP of 1200 mm (1981–2010 climate normals; http://ncdc.noaa.gov).

Non-permineralized wood in the posteruptive Giraffe sequence has exceptional preservation and can be assigned unambiguously to *Metasequoia* on the basis of xylotomy (Fig. DR1). This wood yields pristine α-cellulose (Fig. DR3) amenable to measurements of stable oxygen isotope ratios ($\delta^{18}O_{cell}$) by pyrolysis and continuous-flow isotope ratio mass spectrometry, which in turn can provide independent support for palynological estimates of MAT (Appendix DR1). The values of $\delta^{18}O_{cell}$ range from 23.4‰ to 24.9‰ VSMOW (Vienna standard mean ocean water) (Fig. 2D; Table DR3). Using a Monte Carlo implementation of the Anderson et al. (2002) leaf-water model, we estimated values of $\delta^{18}O$ for environmental waters ($\delta^{18}O_{water}$) accessed by the trees, and then calculated MAT from these inferred $\delta^{18}O_{water}$ values using an empirical relation between Eocene environmental waters and MAT that accounts for Eocene latitudinal temperature gradients (Fricke and Wing, 2004). The $\delta^{18}O_{cell}$ results yield a MAT estimate of 15.6 ± 2.0 °C at 1σ (Fig. 2E), which overlaps the pollen-based MCR estimate of 14.5 ± 1.3 °C MAT (Fig. DR4).

Atmospheric CO$_2$ Reconstruction

Stomatal indices derived from Giraffe *Metasequoia* leaves (Doria et al., 2011) yield a combined median reconstructed atmospheric CO$_2$ concentration for all stratigraphic levels of ~630 ppm (433–1124 ppm at 68% confidence) (Figs. 2F and 3; Table DR4). Combined CO$_2$ estimates from the Franks et al. (2014) gas-exchange model, applied to the same foliage (Appendix DR1), are somewhat lower, ranging from 353 to 561 ppm at 68% confidence with a median of ~430 ppm (Fig. 3A). Given overlap between the two methods of CO$_2$ reconstruction, and because the stomatal index proxy is unbounded at high CO$_2$ concentrations (Doria et al., 2011), we resampled randomly from the combined stomatal index and gas-exchange model reconstructions to yield a consensus median CO$_2$ concentration of ~490 ppm (378–778 ppm at 68% confidence). This approach reduces biases inherent to either technique.

This CO$_2$ reconstruction is lower than inferences of ~800–1000 ppm from alkenone $\delta^{13}C$ between 39 and 37 Ma (Zhang et al., 2013) and 650 ± 110 ppm (at 68% confidence) at 40.3 Ma from $\delta^{11}B$ of pristine foraminiferal calcite (Anagnostou et al., 2016), but in agreement with estimates of 385–467 ppm (at 68% confidence) from the stomatal distributions of Canadian High Arctic *Metasequoia* foliage dating broadly to between 47.9 and 37.8 Ma (Maxbauer et al., 2014) and ~350–650 ppm from the stomatal density of extinct fagalean foliage (Steinthorsdottir et al., 2016). The results from the Giraffe locality thus support lower CO$_2$ concentrations than previously envisaged for greenhouse climate intervals (Franks et al., 2014).

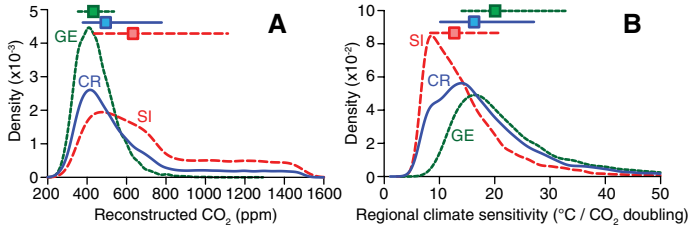

Figure 3. A: Probability density functions (PDFs) for reconstructed CO$_2$ concentrations from *Metasequoia* stomatal index (SI), gas-exchange modeling (GE), and random resampling of the combined stomatal index and gas-exchange model reconstructions (CR). B: PDFs for regional climate sensitivity at the Giraffe locality, subarctic Canada (Appendix DR1 [see footnote 1]). In both panels, horizontal lines indicate the 16th to 84th percentile range, with median values marked by squares.

DISCUSSION

High Polar Amplification under Modest CO_2 Forcing

These data provide an integrated estimate of the mean climate state for the continental subarctic Giraffe locality over the multimillennial interval common to all proxies. The MCR-inferred paleotemperature and reconstructed CO_2 concentrations can be plotted along a range of estimates for the sensitivity of MAT with respect to atmospheric CO_2 (Fig. 4). Present-day estimates of global Charney climate sensitivity (CS) include a subset of fast feedbacks only, while Earth-system sensitivity (ESS) includes most fast and slow feedbacks (Royer, 2016). CS and ESS are typically expressed as globally averaged approximations of the temperature response to incremental CO_2 doublings, expressed as ΔMAT relative to preindustrial conditions. However, recent studies have demonstrated the utility of regional approximations for these parameters (Dyez and Ravelo, 2013; Eagle et al., 2013).

The latest middle Eocene MAT and stomatal index CO_2 reconstruction from Giraffe, when compared to the present climate of Yellowknife using the approach of Royer et al. (2012), yield a mean regional climate sensitivity of 12.7 °C per CO_2 doubling for the North American subarctic latitudes (8.3–21.2 °C at 68% confidence; Fig. 3; Appendix DR1), more than twice the estimated ESS of ~6 °C per CO_2 doubling for the Pleistocene climate system (Hansen et al., 2008; Fig. 4). Use of CO_2 estimates from the gas-exchange model produces even higher regional climate sensitivity values (14.0–32.8 °C at 68% confidence, median = 20.1 °C; Fig. 3).

These estimates of regional climate sensitivity, based on paleoclimate and CO_2 proxies analyzed in parallel from the same sediment archive, highlight the exceptional magnitude of polar amplification under relatively modest CO_2 forcing. This contention is supported by temperature reconstructions from Ellesmere Island and Siberia during the Pliocene (Ballantyne et al., 2010; Brigham-Grette et al., 2013), for which independent proxies (e.g., Zhang et al., 2013) indicate CO_2 concentrations of ~400 ppm (Fig. 4). Even greater ΔMATs (~32 °C) are estimated from middle Eocene fossil floras of Axel Heiberg Island (Eberle and Greenwood, 2012), also dominated by *Metasequoia*, when CO_2 was possibly as low as ~420 ppm (Maxbauer et al., 2014). Pronounced middle Eocene polar amplification is likewise expressed in the Southern Hemisphere high latitudes, where temperate rainforests dominated by *Nothofagus* and araucarian conifers existed along the Wilkes Land margin of East Antarctica, implying MATs >10 °C and MAPs severalfold higher than present (Pross et al., 2012).

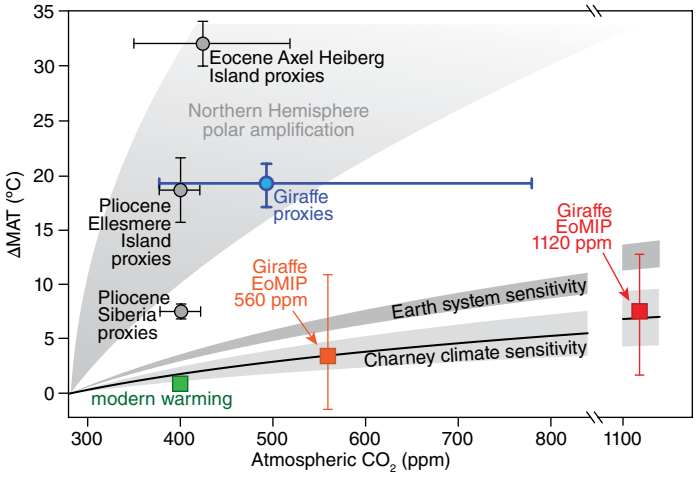

Figure 4. Climate responses to elevated atmospheric CO_2 concentrations. Global estimates of Charney climate sensitivity (CS) and Earth-system sensitivity (ESS) are depicted as light and dark gray envelopes, respectively, with change in mean annual temperature (ΔMAT) plotted relative to preindustrial. CS is after Rohling et al. (2012); upper and lower bounds of the ESS envelope represent ESS/CS ratios of 2.0 estimated for the Pleistocene (Hansen et al., 2008) and 1.65 for the Pliocene (Lunt et al., 2012b). Together with contemporary global MAT at 400 ppm CO_2 (green square), these global estimates provide a context to evaluate polar amplification as recorded by proxy estimates of ΔMAT, relative to present MAT at the nearest climate station, for the Giraffe locality (subarctic Canada; blue circle; combined resampled CO_2 median) and other high-latitude sites (gray circles) for the Pliocene (Ballantyne et al., 2010; Brigham-Grette et al., 2013) and Eocene (Maxbauer et al., 2014). Errors are the 16th to 84th percentile range for the Giraffe locality and 1σ confidence interval for other sites. Model ensemble mean ΔMATs for the Giraffe region (computed relative to present Yellowknife MAT) at 2× and 4× pre-industrial CO_2 (EoMIP; Lunt et al., 2012a) are marked by orange and red squares, respectively; bars mark the range of modeled ΔMAT for each ensemble.

Early Eocene climate model simulations for the latitudes of subarctic North America (Lunt et al., 2012a; Carmichael et al., 2016) underestimate the multiple proxy constraints presented here. For example, at 560 ppm CO_2, the ensemble mean of three models (Lunt et al., 2012a) for the Giraffe region underestimates reconstructed MAT by 15.5 °C, with a minimum underestimate of 6.4 °C (Fig. 4). At 1120 ppm CO_2, more than twice the inferred CO_2 from *Metasequoia* foliage, the ensemble mean MAT is 11.3 °C lower than proxy MATs, with a minimum underestimate of 4.5 °C (Fig. 4). The model results compiled by Lunt et al. (2012a) consistently estimated colder-than-present preindustrial Yellowknife MATs in 280 ppm CO_2 control runs. However, even when this model-dependent artifact is taken into account by expressing ΔMAT relative to instrumental Yellowknife MAT (Fig. DR5), model ΔMATs remain substantially lower than the proxy-based ΔMATs presented here for the Giraffe region (Table DR5).

Many mechanisms have been explored to explain the amplified warmth of high latitudes during the Cretaceous and Paleogene, including state-dependent CS (Caballero and Huber, 2013), decreased atmospheric pressure (Poulsen et al., 2015), altered cloud physics (Kiehl and Shields, 2013), biogenic aerosols (Beerling et al., 2011), and teleconnection dynamics with tropical oceans (Korty et al., 2008). Changes in atmospheric circulation such that low pressure centers and associated cyclogenesis became quasi-permanent features over the polar regions in the absence of perennial sea ice cover were also probable. Such configurations appear necessary to increase MAP by the amounts mandated by the proxy record at Giraffe and elsewhere, whereas intensification of the hydrologic cycle also increases poleward heat transfer by water vapor (Pagani et al., 2014; Carmichael et al., 2016). Despite obvious differences in boundary conditions with respect to the state of the cryosphere and biosphere, these configurations provide some degree of analogy with contemporary warming of the Arctic, where dramatic losses of Northern Hemisphere sea ice over the last decade have contributed to deepening lows over the Arctic Ocean, coupled to enhanced cyclogenesis that in turn exerts a strong positive feedback on remaining sea ice (Screen et al., 2011; Simmonds and Rudeva, 2012).

Because future temperatures are unlikely to decline appreciably over the time scales required for most fast and slow feedbacks to become fully expressed (centuries to millennia; Royer, 2016), even if all anthropogenic greenhouse gas emissions are eliminated (Archer and Brovkin, 2008), the latest middle Eocene forest ecosystem preserved in the Giraffe kimberlite offers considerable insight toward understanding high-latitude climate states under elevated, but not extreme, atmospheric CO_2 concentrations.

ACKNOWLEDGMENTS

We thank BHP Billiton Inc. and the Geological Survey of Canada for access to cores; the Natural Sciences and Engineering Research Council (Canada) (Greenwood, Reyes, Westgate, and Wolfe); the U.S. National Science Foundation (Siver); J. Basinger for discussions on *Metasequoia*; G. Braybrook for scanning electron microscopy; the Climate Change Consortium of Wales, D. McCarroll, and N. Loader for assistance with stable isotopes; R. Zetter for advice on pollen morphology; and G. Ludvigson, M. Steinthorsdottir, B. Jacobs, and several other anonymous reviewers. We dedicate this paper to our departed colleagues Leo Hickey (1940–2013) and Mark Pagani (1960–2016), who trailblazed much of our thought concerning greenhouse worlds of the past, and Art Sweet (1942–2017), pillar of Canadian palynology and the first to analyze Giraffe pipe pollen.

REFERENCES CITED

Anagnostou, E., John, E.H., Edgar, K.M., Foster, G.L., Ridgwell, A., Inglis, G.N., Pancost, R.D., Lunt, D.J., and Pearson, P.N., 2016, Changing atmospheric CO_2 concentration was the primary driver of early Cenozoic climate: Nature, v. 533, p. 380–384, doi:10.1038/nature17423.

Anderson, W.T., Bernasconi, S.M., McKenzie, J.A., Saurer, M., and Schweingruber, F., 2002, Model evaluation for reconstructing the oxygen isotopic composition in precipitation from tree ring cellulose over the last century: Chemical Geology, v. 182, p. 121–137, doi:10.1016/S0009-2541(01)00285-6.

Archer, D., and Brovkin, V., 2008, The millennial atmospheric lifetime of anthropogenic CO_2: Climatic Change, v. 90, p. 283–297, doi:10.1007/s10584-008-9413-1.

Ballantyne, A.P., Greenwood, D.R., Sinninghe Damsté, J.S., Csank, A.Z., Eberle, J.J., and Rybczynski, N., 2010, Significantly warmer Arctic surface temperatures during the Pliocene indicated by multiple independent proxies: Geology, v. 38, p. 603–606, doi:10.1130/G30815.1.

Beerling, D.J., Fox, A., Stevenson, D.S., and Valdes, P.J., 2011, Enhanced chemistry-climate feedbacks in past greenhouse worlds: Proceedings of the National Academy of Sciences of the United States of America, v. 108, p. 9770–9775, doi:10.1073/pnas.1102409108.

Brigham-Grette, J., et al., 2013, Pliocene warmth, polar amplification, and stepped Pleistocene cooling recorded in NE Arctic Russia: Science, v. 340, p. 1421–1427, doi:10.1126/science.1233137.

Caballero, R., and Huber, M., 2013, State-dependent climate sensitivity in past warm climates and its implications for future climate projections: Proceedings of the National Academy of Sciences of the United States of America, v. 110, p. 14162–14167, doi:10.1073/pnas.1303365110.

Carmichael, M.J., et al., 2016, A model-model and data-model comparison for the early Eocene hydrological cycle: Climate of the Past, v. 12, p. 455–481, doi:10.5194/cp-12-455-2016.

Creaser, R., Grütter, H., Carlson, J., and Crawford, B., 2004, Macrocrystal phlogopite Rb-Sr dates for the Ekati property kimberlites: Evidence for multiple intrusive episodes during Paleocene and Eocene time: Lithos, v. 76, p. 399–414, doi:10.1016/j.lithos.2004.03.039.

Doria, G., Royer, D.L., Wolfe, A.P., Fox, A., Westgate, J.A., and Beerling, D.J., 2011, Declining atmospheric CO_2 during the late Middle Eocene climate transition: American Journal of Science, v. 311, p. 63–75, doi:10.2475/01.2011.03.

Dyez, K.A., and Ravelo, A.C., 2013, Late Pleistocene tropical Pacific temperature sensitivity to radiative greenhouse gas forcing: Geology, v. 41, p. 23–26, doi:10.1130/G33425.1.

Eagle, R.A., Risi, C., Mitchell, J.L., Eiler, J.M., Seibt, U., Neelin, J.D., Li, G., and Tripati, A.K., 2013, High regional climate sensitivity over continental China constrained by glacial-recent changes in temperature and the hydrological cycle: Proceedings of the National Academy of Sciences of the United States of America, v. 110, p. 8813–8818, doi:10.1073/pnas.1213366110.

Eberle, J.J., and Greenwood, D.R., 2012, Life at the top of the greenhouse Eocene world—A review of the Eocene flora and vertebrate fauna from Canada's High Arctic: Geological Society of America Bulletin, v. 124, p. 3–23, doi:10.1130/B30571.1.

Franks, P.J., Royer, D.L., Beerling, D.J., Van de Water, P.K., Cantrill, D.J., Barbour, M.M., and Berry, J.A., 2014, New constraints on atmospheric CO_2 concentration for the Phanerozoic: Geophysical Research Letters, v. 41, p. 4685–4694, doi:10.1002/2014GL060457.

Fricke, H.C., and Wing, S.L., 2004, Oxygen isotope and paleobotanical estimates of temperature and $\delta^{18}O$-latitude gradients over North America during the early Eocene: American Journal of Science, v. 304, p. 612–635, doi:10.2475/ajs.304.7.612.

Hansen, J., Sato, M., Kharecha, P., Beerling, D., Berner, R., Masson-Delmotte, V., Pagani, M., Raymo, M., Royer, D.L., and Zachos, J.C., 2008, Target atmospheric CO_2: Where should humanity aim?: Open Atmospheric Science Journal, v. 2, p. 217–231, doi:10.2174/1874282300802010217.

Jagniecki, E.A., Lowenstein, T.K., Jenkins, D.M., and Demicco, R.V., 2015, Eocene atmospheric CO_2 from the nahcolite proxy: Geology, v. 43, p. 1075–1078, doi:10.1130/G36886.1.

Kiehl, J.T., and Shields, C.A., 2013, Sensitivity of the Palaeocene–Eocene thermal maximum climate to cloud properties: Philosophical Transactions of the Royal Society A, v. 371, 20130093, doi:10.1098/rsta.2013.0093.

Korty, R.L., Emanuel, K.A., and Scott, J.R., 2008, Tropical cyclone-induced upper-ocean mixing and climate: Application to equable climates: Journal of Climate, v. 21, p. 638–654, doi:10.1175/2007JCLI1659.1.

Lunt, D.J., et al., 2012a, A model-data comparison for a multi-model ensemble of early Eocene atmosphere–ocean simulations: EoMIP: Climate of the Past, v. 8, p. 1717–1736, doi:10.5194/cp-8-1717-2012.

Lunt, D.J., Haywood, A.M., Schmidt, G.A., Salzmann, U., Valdes, P., Dowsett, H.J., and Lopston, C.A., 2012b, On the causes of mid-Pliocene warmth and polar amplification: Earth and Planetary Science Letters, v. 321–322, p. 128–138, doi:10.1016/j.epsl.2011.12.042.

Maxbauer, D.P., Royer, D.L., and LePage, B.A., 2014, High Arctic forests during the middle Eocene supported by moderate levels of atmospheric CO_2: Geology, v. 42, p. 1027–1030, doi:10.1130/G36014.1.

Pagani, M., Zachos, J.C., Freeman, K.H., Tipple, B., and Bohaty, S., 2005, Marked decline in atmospheric carbon dioxide concentrations during the Paleogene: Science, v. 309, p. 600–603, doi:10.1126/science.1110063.

Pagani, M., Huber, M., and Sageman, B., 2014, Greenhouse climates, *in* Holland, H.D., and Turekian, K.K., eds., Treatise on geochemistry (second edition): Oxford, UK, Elsevier, p. 281–304, doi:10.1016/B978-0-08-095975-7.01314-0.

Poulsen, C.J., Tabor, C., and White, J.D., 2015, Long-term climate forcing by atmospheric oxygen concentrations: Science, v. 348, p. 1238–1241, doi:10.1126/science.1260670.

Pross, J., et al., 2012, Persistent near-tropical warmth on the Antarctic continent during the early Eocene epoch: Nature, v. 488, p. 73–77, doi:10.1038/nature11300.

Rohling, E.J., et al., 2012, Making sense of palaeoclimate sensitivity: Nature, v. 491, p. 683–691, doi:10.1038/nature11574.

Royer, D.L., 2006, CO_2-forced climate thresholds during the Phanerozoic: Geochimica et Cosmochimica Acta, v. 70, p. 5665–5675, doi:10.1016/j.gca.2005.11.031.

Royer, D.L., 2016, Climate sensitivity in the geological past: Annual Review of Earth and Planetary Sciences, v. 44, p. 277–293, doi:10.1146/annurev-earth-100815-024150.

Royer, D.L., Pagani, M., and Beerling, D.J., 2012, Geobiological constraints on Earth system sensitivity to CO_2 during the Cretaceous and Cenozoic: Geobiology, v. 10, p. 298–310, doi:10.1111/j.1472-4669.2012.00320.x.

Screen, J.A., Simmonds, I., and Keay, K., 2011, Dramatic interannual changes of perennial Arctic sea ice linked to abnormal summer storm activity: Journal of Geophysical Research, v. 116, D15105, doi:10.1029/2011JD015847.

Simmonds, I., and Rudeva, I., 2012, The great Arctic cyclone of August 2012: Geophysical Research Letters, v. 39, L23709, doi:10.1029/2012GL054259.

Steinthorsdottir, M., Porter, A.S., Holohan, A., Kunzmann, L., Collinson, M., and McElwain, J.C., 2016, Fossil plant stomata indicate decreasing atmospheric CO_2 prior to the Eocene-Oligocene boundary: Climate of the Past, v. 12, p. 439–454, doi:10.5194/cp-12-439-2016.

Thompson, R.S., Anderson, K.H., Pelltier, R.T., Strickland, L.E., Bartlein, P.J., and Shafer, S.L., 2012, Quantitative estimation of climatic parameters from vegetation data in North America by the mutual climatic range technique: Quaternary Science Reviews, v. 51, p. 18–39, doi:10.1016/j.quascirev.2012.07.003.

Tripati, A.K., et al., 2008, Evidence for Northern Hemisphere glaciation back to 44 Ma from ice-rafted debris in the Greenland Sea: Earth and Planetary Science Letters, v. 265, p. 112–122, doi:10.1016/j.epsl.2007.09.045.

Westgate, J.A., Naeser, N.D., and Alloway, B., 2013, Fission-track dating, *in* Elias, S.A., and Mock, C.J., eds., Encyclopedia of Quaternary science (second edition): Amsterdam, Elsevier, p. 643–662, doi:10.1016/B978-0-444-53643-3.00039-X.

Wolfe, A.P., Edlund, M.B., Sweet, A.R., and Creighton, S.D., 2006, A first account of organelle preservation in Eocene nonmarine diatoms: observations and paleobiological implications: Palaios, v. 21, p. 298–304, doi:10.2110/palo.2005.p05-14e.

Zachos, J.C., Dickens, G.R., and Zeebe, R.E., 2008, An early Cenozoic perspective on greenhouse warming and carbon-cycle dynamics: Nature, v. 451, p. 279–283, doi:10.1038/nature06588.

Zhang, Y.G., Pagani, M., Liu, Z., Bohaty, S.M., and DeConto, R.A., 2013, A 40-million-year history of atmospheric CO_2: Philosophical Transactions of the Royal Society A, v. 371, 20130096, doi:10.1098/rsta.2013.0096.

Manuscript received 29 January 2017
Revised manuscript received 3 March 2017
Manuscript accepted 17 March 2017

Printed in USA